



## Original Research Paper

# Analysis of constant-volume shear tests based on precise measurement of stresses in powder beds



Yasuhiro Shimada, Takumu Kawata, Shuji Matsusaka\*

Department of Chemical Engineering, Kyoto University, Kyoto 615-8510, Japan

## ARTICLE INFO

## Article history:

Received 18 October 2017

Received in revised form 19 February 2018

Accepted 26 February 2018

Available online 8 March 2018

## Keywords:

Powder flowability

Shear test

Powder yield locus

Critical state line

Flow function

## ABSTRACT

This study demonstrates a new constant-volume shear test configuration to analyze the stresses in powder beds and evaluate powder flowability. A novel cylindrical shear cell geometry and load cell arrangement allowed precise measurement of the normal stress acting on the shear planes of the powder beds. The stress transmission ratio between the top and shear planes decreased with increasing ratio of the powder bed height in the upper section of the shear cell to the shear cell diameter. This was due to friction between the powder bed and the side wall of the upper section of the shear cell. Using the measured values of the normal stress on the shear planes, the effects of the powder bed height and shear cell diameter were eliminated from the data. In addition, to evaluate the shear properties of the powder beds, the powder yield locus, consolidation yield locus, critical state line, shear cohesion, and void fraction were obtained from a single shear test. The powder yield locus data were used to obtain flow functions.

© 2018 The Society of Powder Technology Japan. Published by Elsevier B.V. and The Society of Powder Technology Japan. This is an open access article under the CC BY-NC-ND license (<http://creativecommons.org/licenses/by-nc-nd/4.0/>).

## 1. Introduction

In recent years, particle size reduction has become increasingly popular in various industries to improve the quality and performance of functional particles. However, small particles easily adhere and have low flowability, which causes problems related to powder handling in the development of new products and quality control of industrial processes. Appropriately evaluating powder flowability to resolve these issues remains challenging; many characteristic properties of particles, e.g., particle size distribution, particle density, particle shape, and specific surface area, affect the powder flow behavior in a complicated manner. Consequently, it is difficult to accurately predict the powder flowability even if all relevant characteristics can be quantified.

To quantitatively evaluate powder flowability, various methods and characteristic values have been proposed, e.g., the angle of repose, bulk density, compressibility, tensile strength, and shear strength; however, these values do not always lead to the same results. To comprehensively evaluate powder flowability, Carr [1] proposed a series of indices that correspond to different flow phenomena, i.e., the angle of repose, compressibility, angle of spatula, and cohesion or uniformity. This method is effective for evaluating the powder flowability under low stress. In addition, the avalanche

method [2], vibratory feeder method [3], vibrating tube method [4,5], and vibration shear tube method [6] are effective for similar conditions as the applied forces are rather small.

On the other hand, for large stresses, the flowability depends on the magnitude of the applied stress. Hence, it is necessary to precisely measure such stresses and shear tests have been used for this purpose. Such test methods can be classified into several types depending on the structure of the shear cell, such as the Jenike cell [7,8] and rotational shear cell [9–11]. In addition, standards for the measurement and evaluation methods have been developed [12–15]. These shear tests have been employed in research in various industrial fields, e.g., the food industry, to measure the effect of moisture content [16,17], storage time [18], and particle shape [19,20], on the flowability, and in the pharmaceutical field for tableting [21] and prescription design [22]. The results of such shear tests are often used to design silos and hoppers [23] as a large amount of powder is naturally consolidated by gravity in such applications. In materials research, the flowability of nanoparticles has been analyzed [24].

Several developments have been made to both shear test equipment [25] and analytical methods [26,27], allowing use of the technique in expanded application areas. In the Jenike shear tester, the normal stress on the powder bed is determined by a weight placed on top of the powder and the normal stress on the horizontal cross-sectional area decreases due to the friction between the powder bed and the side wall of the shear cell. Therefore, the normal stress

\* Corresponding author.

E-mail address: [matsu@cheme.kyoto-u.ac.jp](mailto:matsu@cheme.kyoto-u.ac.jp) (S. Matsusaka).

**Nomenclature**

$A_P$	horizontal cross-sectional area of powder bed ( $m^2$ )	$\gamma_{TD}$	stress transmission ratio between top and shear planes at steady-state shear, i.e., point D (-)
$A_L$	area of side of powder bed in lower section of shear cell ( $m^2$ )	$\varepsilon$	void fraction (-)
$A_U$	area of side of powder bed in upper section of shear cell ( $m^2$ )	$\rho_b$	bulk density ( $kg/m^3$ )
$C$	shear cohesion (Pa)	$\sigma$	normal stress (Pa)
$D_C$	inner diameter of shear cell (m)	$\sigma_1$	major principal stress given by the Mohr stress circle of steady state flow (Pa)
$D_{p50}$	mass median diameter of powder (m)	$\sigma_g$	geometric standard deviation of particle diameter (-)
$F$	force (N)	$\tau$	shear stress (Pa)
$FF$	flow function (Pa)	$\varphi_{CSL}$	angle of critical state line ( $^\circ$ )
$f_c$	unconfined yield strength (Pa)		
$ff_c$	$=\sigma_1/f_c$ (-)		
$g$	acceleration due to gravity ( $m/s^2$ )	<b>Subscripts</b>	
$H_{PU}$	powder bed height in upper section of shear cell (m)	C	cell
$k$	constant in Eq. (6) (-)	E	point E (steady-state shear)
$\Delta L_H$	horizontal shear displacement (m)	H	horizontal
$M_B$	mass of base (kg)	L	lower
$M_{BP}$	mass of bottom plate (kg)	P	powder
$M_P$	mass of powder (kg)	S	shear plane
$t$	time (s)	U	upper
		V	vertical

on the shear plane is not equal to the value calculated simply from the weight and the cross-sectional area. In a previous study [28], we used a constant-volume shear tester and proposed a method for measuring vertical forces acting on both the bottom and top of the shear cell; however, the stresses in the powder beds were not studied in detail.

In the present study, the effect of powder bed height and shear cell diameter on the stresses was investigated and the validity of the constant-volume shear tests based on the normal stress on the shear plane was verified. In addition, the powder yield locus (PYL), consolidation yield locus (CYL), critical state line (CSL), shear cohesion, and void fraction were obtained under various conditions to evaluate the shear properties of the powder beds. Furthermore, the PYL data were used to obtain flow functions.

**2. Materials and methods**

**2.1. Constant-volume shear test apparatus**

Fig. 1 shows schematic diagrams of the two types of common shear test methods, i.e., the constant-load and constant-volume

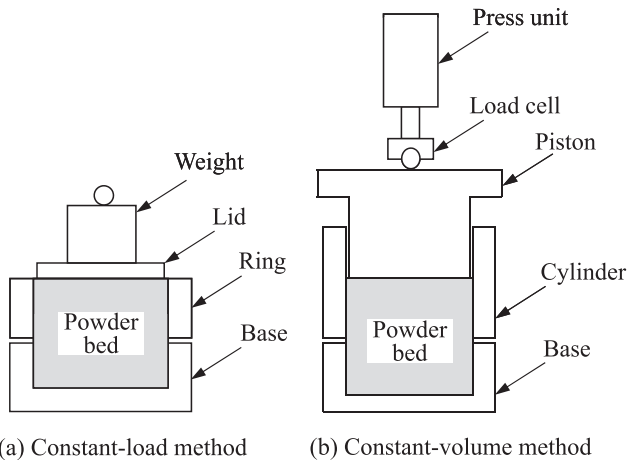


**Fig. 1.** Schematic diagram showing two types of shear test methods. (a) Constant-load method. (b) Constant-volume method.

methods. The former uses a weight to apply a constant normal stress to the top plane of the powder bed, while the latter uses a mechanical press, where the vertical position of the top plane of the powder bed is fixed during the shear test.

Fig. 2 schematically illustrates the shear stress ( $\tau$ ) obtained from the constant-volume test as a function of the normal stress ( $\sigma$ ) and the void fraction ( $\varepsilon$ ) [29]. When shearing at a constant velocity starts from point D, the normal stress decreases and the shear stress increases; however, these stresses approach their respective constant values at point E, which indicates steady-state shear on the critical state line (CSL). After this point, by gradually lowering the base of the shear cell, where there is little change ( $\leq 0.5\%$ ) in the void fraction of the powder bed, both the shear stress and normal stress decrease (moving along the curve from point E to point C). Therefore, by continuously measuring  $\tau$

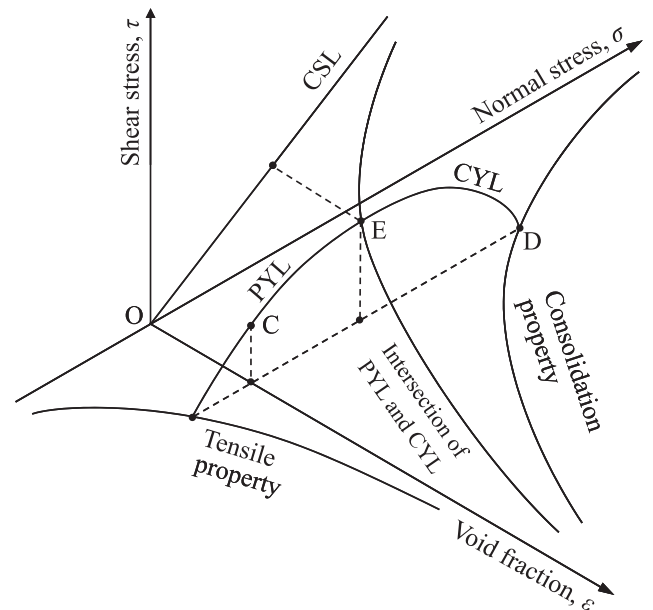


**Fig. 2.** A three-dimensional diagram showing the relationships between the mechanical properties of a powder bed.

and  $\sigma$  during the shearing process, a relationship between these two factors, i.e., the powder yield locus (PYL), is obtained. The PYL describes the characteristics of the failure of the powder bed under low normal stress. The characteristics of failure under high normal stress are indicated by the curve between points D and E, the consolidation yield locus (CYL). Therefore, complete behavior of the powder bed can be characterized by determining the two yield loci.

## 2.2. Experimental apparatus

Fig. 3 shows a schematic diagram of the experimental apparatus. The inner diameters (cell diameter  $D_C$ ) of the stainless steel cylindrical shear cells with separate upper and lower sections were 15, 30, and 43 mm. The cylindrical upper section was fixed and the lower section moved horizontally to induce shearing. The edges of the cylindrical upper section and the lower section were separated by a narrow gap (0.2 mm), and when not filled with powder, the horizontal movement produced a very small amount of friction on the lower section (less than 0.3 kPa, which is thought to be insignificant compared to the stress applied during the shear test). The upper part of the setup featured a vertical servo motor to move the upper layers of the powder bed downward. The vertical force acting on the top of the shear cell, the vertical force acting on the bottom, and the horizontal shear force were measured using load cells. Additionally, the height of the powder bed in the cylindrical upper section and the horizontal shear displacement were measured using non-contact displacement sensors.

## 2.3. Mechanism for measuring normal and shear stress

Fig. 4 shows a schematic diagram of the cell structure of the shear testing apparatus and the stresses acting upon the powder bed when a vertical load was applied. Fig. 4(a) shows the apparatus with a separation between the bottom plate and the side wall of the lower section of the shear cell, while Fig. 4(b) shows a structure where the lower piece of the cell is used as the bottom plate. In both cases, load cells were located in both the upper and lower sections, enabling the measurement of the vertical force acting on the top of the shear cell ( $F_{VU}$ ) and the vertical force acting on the bottom of the shear cell ( $F_{VL}$ ).

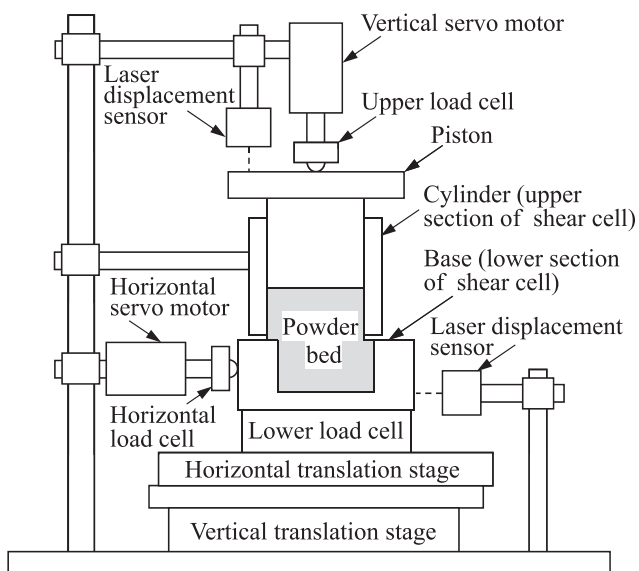


Fig. 3. Schematic diagram showing the experimental apparatus for the constant-volume shear tests.

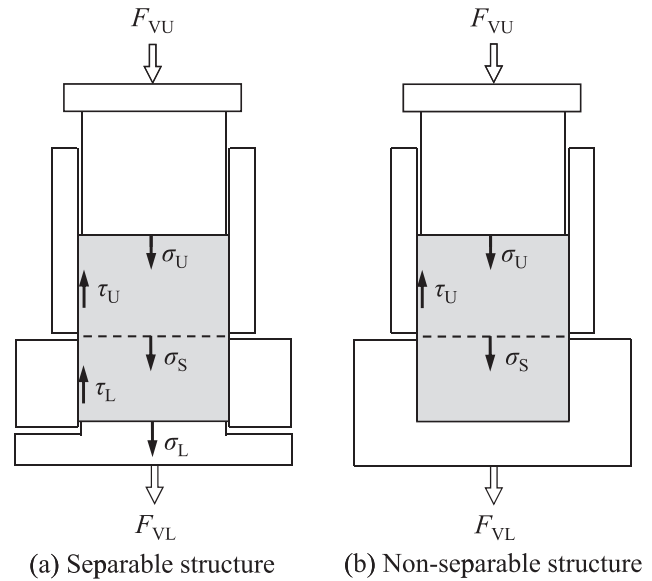


Fig. 4. Schematic diagram showing the two types of shear cells used for constant-volume shear tests.

When the bottom plate is separated, the vertical force ( $F_{VL}$ ) can be expressed as:

$$F_{VL} = F_{VU} + (M_{PU} + M_{PL} + M_{BP})g - \tau_U A_U - \tau_L A_L, \quad (1)$$

where  $M_{PU}$  and  $M_{PL}$  are the masses of the powder filling the upper and lower sections, respectively,  $M_{BP}$  is the mass of the bottom plate,  $g$  is the acceleration due to gravity,  $\tau_U$  and  $\tau_L$  are the friction stresses between the powder bed and the side walls of the shear cell in the upper and lower sections, respectively, and  $A_U$  and  $A_L$  are the areas of the powder bed in contact with the side walls of the shear cell in the upper and lower sections, respectively. Here, the variables  $\tau_U$  and  $\tau_L$  in Eq. (1) were not measured.

When the lower section of the shear cell acts as the bottom plate, the vertical force ( $F_{VL}$ ) is expressed as:

$$F_{VL} = F_{VU} + (M_{PU} + M_{PL} + M_B)g - \tau_U A_U, \quad (2)$$

where  $M_B$  is the mass of the base. The variable  $\tau_U$  in Eq. (2) was not measured, but all other values were known, enabling calculation of this force. The normal stress most relevant to the shear test is not the stress on the top and bottom planes of the powder bed, but rather the stress on the shear plane. The normal stress acting upon the shear plane ( $\sigma_S$ ) is expressed as:

$$\sigma_S = \frac{F_{VU} + M_{PU}g - \tau_U A_U}{A_p}, \quad (3)$$

where  $A_p$  is the horizontal cross-sectional area of the powder bed. By combining Eqs. (2) and (3), the following equation is obtained:

$$\sigma_S = \frac{F_{VL} - (M_{PL} + M_B)g}{A_p}. \quad (4)$$

In other words, when the lower section is used as the bottom plate, the normal stress acting on the shear plane ( $\sigma_S$ ) can be calculated from  $F_{VL}$ , which means that the relationship between the powder bed shear stress ( $\tau_S$ ) and  $\sigma_S$  can be precisely determined. In this work, we decided to use a cell with the lower section acting as a bottom plate.

## 2.4. Sample preparation

White fused alumina abrasive (WA, Fujimi Inc.) was used as the powder in the shear test. WA consists of fused alumina pulverized

into fine particles, and is widely used in precision manufacturing. Table 1 shows the mass median particle diameter ( $D_{p50}$ ) and geometric standard deviation ( $\sigma_g$ ) of the WA powder used. The particle shape was irregular.

## 2.5. Experimental procedure

After loading the sample into the shear cell, the vertical servo motor lowered the top plane of the sample powder bed at 0.2 mm/s to apply pressure to the powder bed. When a set value of  $\sigma_s$  was reached, the movement was stopped and the position was held for a period (maximum 120 s) to relieve the excess stress. During the shear tests, different amounts of powder were filled into the cell to give powder bed heights ( $H_{pu}$ ) of  $10 \pm 1$  mm,  $15 \pm 1$  mm, and  $20 \pm 1$  mm in the upper section. A horizontal servo motor moved the lower section of the shear cell at a set speed ( $10 \mu\text{m/s}$ ) to induce shearing of the powder bed. Once the shear stress reached a critical value, the stage upon which the shear cell rested was gradually lowered until  $\sigma_s$  reached zero to complete the shear test.

## 2.6. Measurements and analytical methods

### 2.6.1. Time sequence of shear test

Fig. 5 shows representative measurement results obtained using shear tests performed with the apparatus shown in Fig. 4 (b). It shows, from top to bottom, the time dependence of variations in the powder bed height in the cylindrical upper section of the shear cell ( $H_{pu}$ ), the horizontal shear displacement ( $\Delta L_H$ ), the vertical force measured by the upper load cell ( $F_{VU}$ ), the vertical force measured by the lower load cell ( $F_{VL}$ ), and the horizontal shear force ( $F_H$ ). After the sample was loaded, the process could be divided into four parts: (i) application of stress to the powder bed by the vertical servo motor, (ii) stress relief after stopping the motor and movement, (iii) powder bed shearing induced by the horizontal servo motor, and (iv) powder bed shearing induced by gradually lowering the stage upon which the shear cell rests, thus decreasing the vertical force. Points C, D, and E in Fig. 5 correspond to those defined in Fig. 2.

During stressing process (i), the stress was applied to the powder bed until  $\sigma_s$  was reached; friction between the powder bed and the side wall of the shear cell resulted in different magnitudes of  $F_{VU}$  and  $F_{VL}$ . The stress relieving process (ii) relieved the excess stress in the powder bed by allowing very small movements of the particles; however, after particle movement ceased,  $F_{VU}$  was not equal to  $F_{VL}$  (point D). In shearing process (iii), the two vertical forces decreased and approached constant values (point E). The horizontal shear force increased up to a certain value due to shearing but then decreased with decreasing vertical force. The purpose of shearing process (iv) was to decrease both the vertical and horizontal forces, where the stage on which the shear cell rested was manually lowered. The variation in the force with time depended on the velocity at which the stage was lowered. However, when the rate of change of normal pressure is less than 10 kPa/s, the shear stress responds well to the normal stress without a time delay. As a result, the velocity of the stage did not affect the

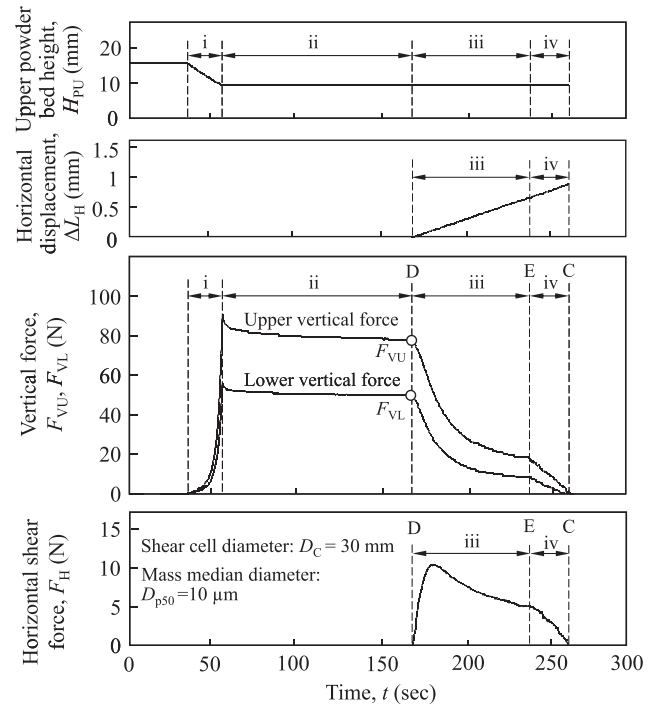


Fig. 5. Time sequence of the shear test.

relationship between the shear and normal stresses, which enabled us to elucidate the inherent properties of the powder.

### 2.6.2. Stress transmission ratio

In the experimental apparatus used here, the cylindrical upper section of the shear cell remained fixed while the lower section moved. Due to the friction between the powder bed and the side wall of the shear cell, the normal stress on the horizontal cross-sectional area decreased with increasing powder bed depth. Here, the stress transmission ratio between the top plane and the shear plane ( $\gamma_{TD}$ ) after stress relief (point D) was calculated from  $\sigma_s$  and the normal stress on the top plane of the powder bed ( $\sigma_U = F_{VU}/A_p$ ), i.e.,

$$\gamma_{TD} = \frac{\sigma_s}{\sigma_U}. \quad (5)$$

Applying Janssen's theoretical model [30] to the powder bed, where the effect of its weight is negligible (less than 1% under the experimental conditions), the stress transmission ratio is expressed as:

$$\gamma_{TD} = \exp\left(-k \frac{H_{pu}}{D_C}\right), \quad (6)$$

where  $k$  is a dimensionless constant. Hence, the stress transmission ratio can be calculated from the ratio of  $H_{pu}$  to  $D_C$ .

### 2.6.3. CYL, PYL, and CSL

The value  $\tau_s$  can be determined by dividing  $F_H$  by  $A_p$ . Further,  $\sigma_s$  can be determined by substituting  $F_{VL}$  into Eq. (4). The relationship between  $\tau_s$  and  $\sigma_s$  over time between points D and E corresponds to the CYL, and the relationship between  $\tau_s$  and  $\sigma_s$  between points E and C corresponds to the PYL. In addition, the straight line connecting point E and the origin corresponds to CSL.

### 2.6.4. Flow function

The powder flowability can be evaluated by a flow function (FF) based on the PYL obtained from the shear test [7], which expresses

Table 1  
Powder properties.

Materials	$D_{p50}$ ( $\mu\text{m}$ )	$\sigma_g$ (-)
Fused alumina #3000	4	1.3
Fused alumina #1200	10	1.2
Fused alumina #280	48	1.2

the relationship between the unconfined yield strength ( $f_c$ ) and the major principal stress given by the Mohr stress circle of steady state flow ( $\sigma_1$ ):

$$ff_c = \frac{\sigma_1}{f_c}, \quad (7)$$

The standards for flowability are the following:  $1 < ff_c < 2$ : very cohesive;  $2 < ff_c < 4$ : cohesive;  $4 < ff_c < 10$ : easy flowing; and  $ff_c > 10$ : free flowing [26].

### 3. Results and discussion

#### 3.1. Stress transmission ratio

Fig. 6 shows the relationship between  $\gamma_{TD}$  and  $H_{PU}$  for samples with different  $D_{p50}$  values. The value of  $\gamma_{TD}$  decreased with increasing  $H_{PU}$ . As  $H_{PU}$  increased, the area of contact between the powder bed and the shear cell wall also increased; thus, the effect of friction increased, resulting in the decrease in  $\gamma_{TD}$ . This figure also depicts the theoretical curves of Eq. (6), as derived from the Jansen model, showing that the experimental results agreed well with the theoretical calculations. The value of  $k$  in Eq. (6) determined by fitting the data was  $2 \pm 0.3$ , and depends on the mechanical properties of the powder bed in the shear cell. However, the effect of particle diameter on  $k$  is not accounted for in this data.

Fig. 7 shows the relationship between  $\gamma_{TD}$  and  $D_C$  for samples with different  $H_{PU}$  values. The value of  $\gamma_{TD}$  increased with increasing  $D_C$  resulting in a decrease in the effect of friction on  $\gamma_{TD}$ , while the  $\gamma_{TD}$  values decreased with increasing  $H_{PU}$ . The experimental data shown in this figure also agreed well with the theoretical curves.

Fig. 8 shows the relationship between  $\gamma_{TD}$  and  $H_{PU}/D_C$ . Since these experimental results agreed well with the theoretical calculations based on  $H_{PU}/D_C$ , we concluded that the value of  $\gamma_{TD}$  can be evaluated using  $H_{PU}/D_C$ . These results show that by decreasing  $H_{PU}$  and/or increasing  $D_C$ , the normal stress in the upper section of the shear cell is effectively transmitted to the shear plane. It is therefore necessary to consider  $H_{PU}/D_C$  when designing the geometry of a cell for experimental shear tests.

#### 3.2. Effect of powder bed height on the YL in the cylindrical section of the shear cell

Fig. 9 shows  $\tau_s$  as a function of  $\sigma_U$  for different  $H_{PU}$  values. To unify the initial condition of shearing,  $\sigma_s$  at the start of shearing was set within a fixed range ( $215 \pm 5$  kPa). As a result,  $\tau_s$  at the

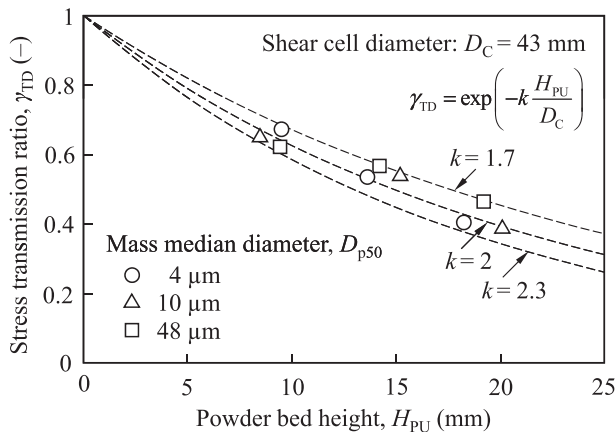


Fig. 6. Effect of powder bed height  $H_{PU}$  in the upper section of the shear cell on the stress transmission ratio  $\gamma_{TD}$  between the top and shear planes at point D.

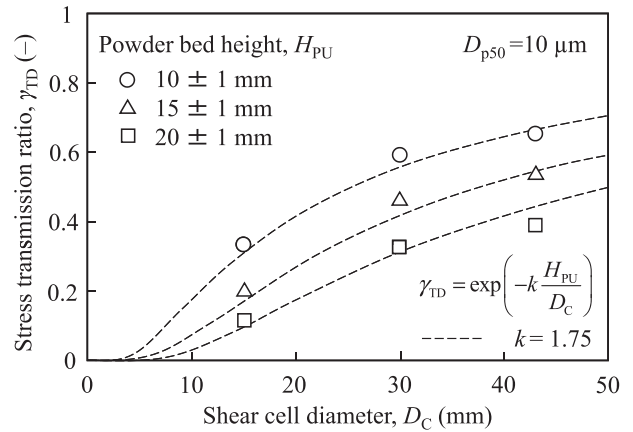


Fig. 7. Effect of the shear cell diameter  $D_C$  on the stress transmission ratio  $\gamma_{TD}$ .

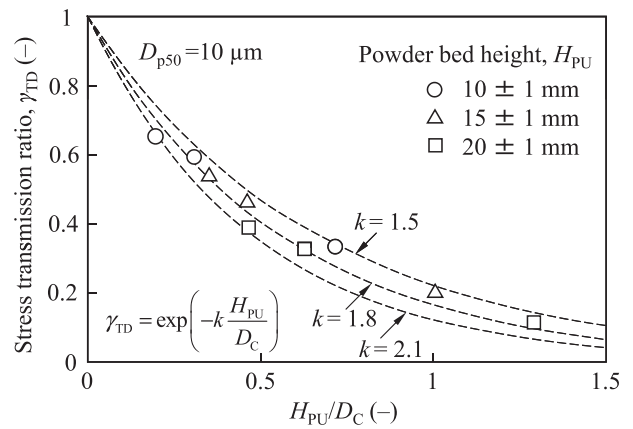


Fig. 8. Effect of the shape of the powder bed  $H_{PU}/D_C$  on the stress transmission ratio  $\gamma_{TD}$ .

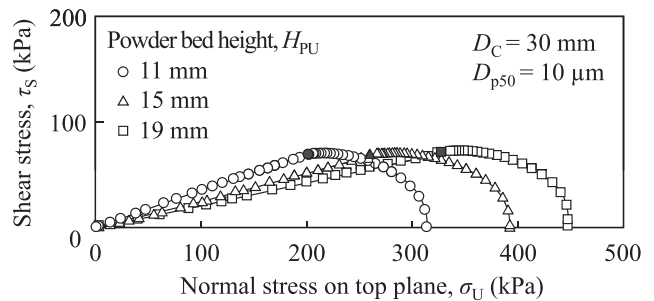


Fig. 9. Shear test results ( $\tau_s$ - $\sigma_U$  plots) at different powder bed heights  $H_{PU}$ .

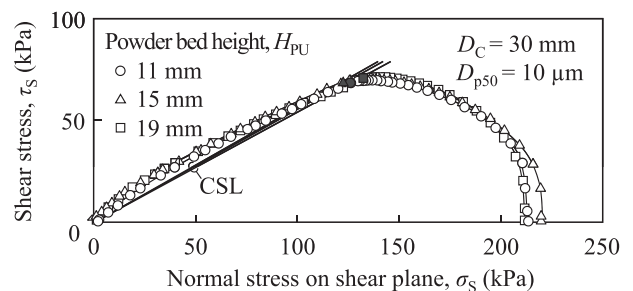


Fig. 10. Shear test results ( $\tau_s$ - $\sigma_s$  plots) at different powder bed heights  $H_{PU}$ .

critical state indicated by point E (marked by black filled data points) was almost constant (70 kPa) irrespective of  $H_{PU}$ . However, for high values of  $H_{PU}$ ,  $\sigma_U$  must also be high considering friction between the powder bed and the shear cell wall. Therefore, there is a large discrepancy in the observed YLs. Since the normal stress at point E could not be determined, the evaluation of the YL as a function of  $\sigma_U$  was not valid.

Fig. 10 shows the results of plotting  $\tau_S$  as a function of  $\sigma_S$  for different  $H_{PU}$  values; these data were obtained from the same shear tests as those shown in Fig. 9. It was found that the YL and CSL values were similar for all  $H_{PU}$  values. Therefore, even when shear tests were conducted with different powder bed heights, analysis of  $\tau_S$  as a function of  $\sigma_S$  is an appropriate method for accurate evaluation of the powder properties.

3.3. Effect of the cell diameter on YL

Fig. 11 shows  $\tau_S$  as a function of  $\sigma_U$  for different  $D_C$  values. The initial  $\sigma_S$  value was set within a fixed range ( $110 \pm 3$  kPa). Since the area of contact between the powder bed and the shear cell wall varied according to the magnitude of  $D_C$ , the effect of friction and the transmissibility of the normal stress also depended on  $D_C$ . In other words, when the cell diameter decreased, the stress transmission ratio also decreased due to the increase in the effect of friction between the powder bed and the shear cell wall. This means that for low  $D_C$  values, a higher  $\sigma_U$  value is required to achieve the same  $\sigma_S$  value, resulting in a large discrepancy in the observed YL values.

Fig. 12 shows  $\tau_S$  as a function of  $\sigma_S$  for different  $D_C$  values, which were obtained from the same shear tests as the data shown in Fig. 11. These YL and CSL values were similar for all cell diameters. Therefore, proper evaluation of the powder properties is possible by conducting shear tests and analyzing  $\tau_S$  as a function of  $\sigma_S$ , irrespective of the  $D_C$  value.

3.4. Effect of the particle diameter on YL

Fig. 13 shows the relationship between  $\tau_S$  and  $\sigma_S$  for two types of powder with different  $D_{p50}$  values (10  $\mu\text{m}$  and 48  $\mu\text{m}$ ). We set  $\sigma_S$  to three different levels and obtained the corresponding PYL and CYL values. The void fraction of the powder beds ( $\epsilon$ ) depended on the initial normal stress, so it needed to be measured for each shear test. YL varied depending on  $\epsilon$ ; the value at the steady-state shear (point E, marked by filled data points) also varied. However, all E points fell along the CSL intersecting the origin. The angle of the CSL corresponds to the angle of dynamic friction, i.e.,  $\varphi_{CSL} = 31^\circ$  for  $D_{p50} = 10 \mu\text{m}$  and  $\varphi_{CSL} = 25^\circ$  for  $D_{p50} = 48 \mu\text{m}$ . This demonstrates that smaller particles show a higher angle of dynamic friction, resulting in poorer powder flow.

3.5. Flow function

Fig. 14 shows the flow functions (solid lines) derived from the results in Section 3.4 and lines of constant flowability ( $ff_c = 1, 2, 4, \text{ and } 10$ , broken lines). The flow function curve for smaller particles exhibited smaller  $ff_c$  values, i.e., lower flowability. Here, it should be noted that using the present constant-volume shear test configuration, we could obtain YL from a single shear test; thus, the flow function can be derived much more easily than demonstrated previously. For reference, the relevant data, i.e., the bulk density  $\rho_b$ , void fraction  $\epsilon$ , shear cohesion  $C$ , angle of dynamic friction of powder  $\varphi_{CSL}$ , major principal stress  $\sigma_1$ , unconfined yield strength  $f_c$ , and the ratio  $ff_c (= \sigma_1/f_c)$  derived from the shear tests for the sample powder, are shown in Table 2.

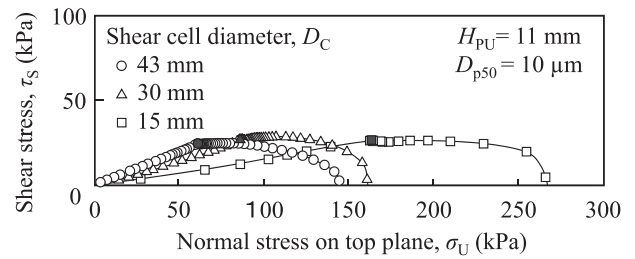


Fig. 11. Shear test results ( $\tau_S$ – $\sigma_U$  plots) at different shear cell diameters  $D_C$ .

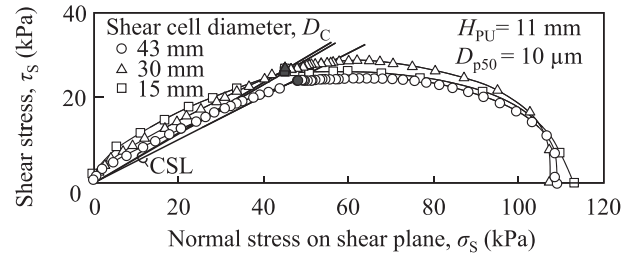


Fig. 12. Shear test results ( $\tau_S$ – $\sigma_S$  plots) at different shear cell diameters  $D_C$ .

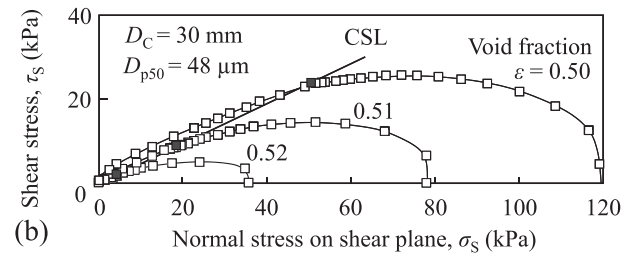
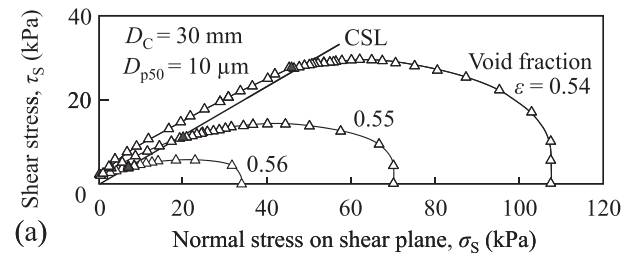


Fig. 13. Shear test results ( $\tau_S$ – $\sigma_S$  plots) at different void fractions  $\epsilon$ . (a)  $D_{p50} = 10 \mu\text{m}$  and (b)  $D_{p50} = 48 \mu\text{m}$ .

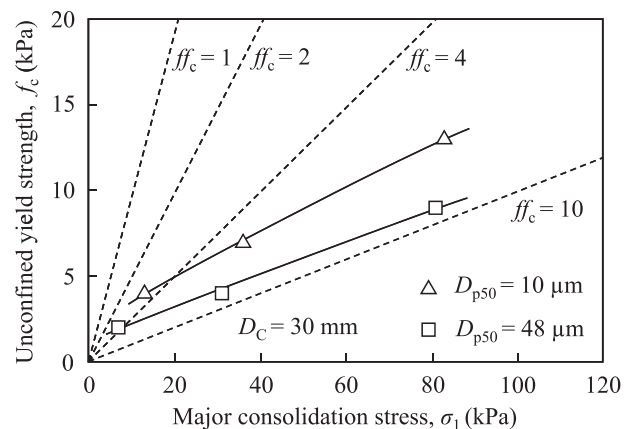


Fig. 14. Flow functions ( $f_c$ – $\sigma_1$  plots) of powders and lines of constant flowability  $ff_c$ .

**Table 2**  
Summary of experimental results for shear tests of powders.

	$\rho_b$ (kg/m <sup>3</sup> )	$\varepsilon$ (–)	C (kPa)	$\varphi_{CSL}$ (°)	$\sigma_1$ (kPa)	$f_c$ (kPa)	$f_c^*$ (–)
Fused alumina (#1200)	1700	0.56	2.3	31	13	4	3.3
$D_{p50} = 10 \mu\text{m}$	1750	0.55	1.8		36	7	5.1
	1790	0.54	2.0		83	13	6.4
Fused alumina (#280)	1860	0.52	0.8	25	7	2	3.5
$D_{p50} = 48 \mu\text{m}$	1910	0.51	0.8		31	4	7.8
	1950	0.50	0.7		81	9	9.0

#### 4. Conclusions

Here we demonstrated a constant-volume shear test apparatus that was able to precisely measure the upper and lower normal stresses of powder beds that allowed us to investigate powder flowability. Using the lower section of the shear cell as the bottom plate enabled measurement of the normal stress on the actual shear plane rather than the normal stress on the top or bottom plane of the powder bed. As the ratio of the powder bed height in the upper section of the shear cell to the shear cell diameter increased, the stress transmission ratio decreased. Evaluating the normal stress on the shear plane, the effects of the shape and/or size of the shear cell were eliminated from the results and reproducible powder flowability behavior was observed.

The proposed experimental method allowed the powder yield locus, consolidation yield locus, critical state line, shear cohesion, powder bed void fraction, and stress transmission ratio to be easily and precisely measured with a single shear test. In addition, shear test data at three levels of normal stress were efficiently obtained, making this method suitable for evaluating the flow function.

#### References

- [1] R.L. Carr, Evaluating flow properties of solids, *Chem. Eng. Jan.* 18 (1965) 163–168.
- [2] F. Lavoie, L. Cartilier, R. Thibert, New methods characterizing avalanche behavior to determine powder flow, *Pharm. Res.* 19 (2002) 887–893.
- [3] S.N. Bhattachar, D.B. Hedden, A.M. Olsofsky, X. Qu, W.Y. Hsieh, K.G. Canter, Evaluation of the vibratory feeder method for assessment of powder flow properties, *Int. J. Pharm.* 269 (2004) 385–392.
- [4] Y. Jiang, S. Matsusaka, H. Masuda, T. Yokoyama, Evaluation of flowability of composite particles and powder mixtures by a vibrating capillary method, *J. Chem. Eng. Jpn.* 39 (2006) 14–21.
- [5] T. Horio, M. Yasuda, S. Matsusaka, Measurement of flowability of lubricated powders by the vibrating tube method, *Drug Dev. Ind. Pharm.* 39 (2013) 1063–1069.
- [6] I.M. Zainuddin, M. Yasuda, T. Horio, S. Matsusaka, Experimental study on powder flowability using vibration shear tube method, *Part. Part. Syst. Charact.* 29 (2012) 8–15.
- [7] A.W. Jenike, Gravity flow of bulk solids, Bulletin No. 108, Utah Engineering Experiment Station, Univ. of Utah, 1961.
- [8] A.W. Jenike, Quantitative design of mass-flow bins, *Powder Technol.* 1 (1967) 237–244.
- [9] J. Schwedes, D. Schulze, Measurement of the flow properties of bulk solids, *Powder Technol.* 61 (1990) 59–68.
- [10] R.J. Berry, M.S.A. Bradley, Investigation of the effect of test procedure factors on the failure loci and derived failure functions obtained from annular shear cells, *Powder Technol.* 174 (2007) 60–63.
- [11] R. Freeman, Measuring the flow properties of consolidated, conditioned and aerated powders - a comparative study using a powder rheometer and a rotational shear cell, *Powder Technol.* 174 (2007) 25–33.
- [12] ASTM D6128, Standard test method for shear testing of bulk solids using the Jenike shear tester.
- [13] ASTM D6773, Standard test method for bulk solids using Schulze ring shear tester.
- [14] JIS Z8835, Direct shear testing method for critical state line (CSL) and wall yield locus (WYL) of powder bed.
- [15] J.W. Carson, H. Wilms, Development of an international standard for shear testing, *Powder Technol.* 167 (2006) 1–9.
- [16] S. Kamath, V.M. Puri, H.B. Manbeck, Flow property measurement using the Jenike cell for wheat flour at various moisture contents and consolidation times, *Powder Technol.* 81 (1994) 293–297.
- [17] V. Karde, D. Dixit, C. Ghoroi, Adhesion force approximation at varying consolidation stresses for fine powder under humid conditions, *Adv. Powder Technol.* 28 (2017) 346–355.
- [18] E. Teunou, J.J. Fitzpatrick, Effect of storage time and consolidation on food powder flowability, *J. Food Eng.* 43 (2000) 97–101.
- [19] W. Yu, K. Muteki, L. Zhang, G. Kim, Prediction of bulk powder flow performance using comprehensive particle size and particle shape distributions, *J. Pharm. Sci.* 100 (2011) 284–293.
- [20] J. Mellmann, T. Hoffmann, C. Füll, Flow properties of crushed grains as a function of the particle shape, *Powder Technol.* 249 (2013) 269–273.
- [21] S. Nakamura, N. Otsuka, Y. Yoshino, T. Sakamoto, H. Yuasa, Predicting the occurrence of sticking during tablet production by shear testing of a pharmaceutical powder, *Chem. Pharm. Bull.* 64 (2016) 512–516.
- [22] Y. Wang, R.D. Snee, W. Meng, F.J. Muzzio, Predicting flow behavior of pharmaceutical blends using shear cell methodology: a quality by design approach, *Powder Technol.* 294 (2016) 22–29.
- [23] S. Jiri, H. Shu-San, C. Yau-Pin, H. Ta-Ching, L. Ti-Chen, Flow patterns and velocity fields in two-dimensional thin slice panel with flow-corrective insert, *Adv. Powder Technol.* 23 (2012) 548–557.
- [24] E. Xanthakisa, J.R. van Ommenb, L. Ahrnéa, Flowability characterization of nanopowders, *Powder Technol.* 286 (2015) 156–163.
- [25] H. Tsunakawa, R. Aoki, Measurements of the failure properties of granular materials and cohesive powders, *Powder Technol.* 33 (1982) 249–256.
- [26] J. Schwedes, Review on testers for measuring flow properties of bulk solid, *Granul. Matter* 5 (2003) 1–43.
- [27] K. Takenaka, K. Iimura, M. Suzuki, M. Hirota, Shape effects of the yield locus on the Rankine coefficient, *Adv. Powder Technol.* 19 (2008) 25–37.
- [28] Y. Shimada, S. Hatano, S. Matsusaka, A new method for evaluating powder flowability using constant volume shear tester, *J. Soc. Powder Technol. Jpn.* 54 (2017) 90–96.
- [29] K.H. Roscoe, A.N. Schofield, C.P. Wroth, On the yielding of soils, *Géotechnique* 8 (1958) 22–53.
- [30] L. Vanel, Ph. Claudin, J.-Ph. Bouchaud, M.E. Cates, E. Clément, J.P. Wittmer, Stresses in silos: comparison between theoretical models and new experiments, *Phys. Rev. Lett.* 84 (2000) 1439–1442.